Autonomous Shape Estimation Using Ranging Sensors

Emily M. Lambert, Weston R. Faber, Islam Nazmy, Islam Hussein
L3Harris – Applied Defense Solutions

ABSTRACT

This paper presents a novel approach to autonomous shape estimation of Resident Space Objects (RSO) using Random Finite Set (RFS) Bayesian estimation and techniques from stochastic optimal control. Estimating RSO shape is a key enabler for many future space operations including space debris removal, satellite diagnostics, and threat assessment and remediation. This paper develops the formulation and approach to the challenge of autonomous shape estimation and illustrates the utility of such systems under non-ideal conditions, e.g. without target RSO illumination or communication with the ground. The results show that the developed solution is able to autonomously estimate the shape of simulated unknown RSO.

Keywords: Space Situational Awareness; Autonomy; Shape Estimation; Guidance Navigation and Control; Random Finite Sets

Acronyms/Abbreviations

ACE – Advanced Composition Explorer
AFOSR – Air Force Office of Scientific Research
DAM – Data Association Matrix
DAP – Data Association Problem
FISST – Finite Set Statistics
FOV – Field of View
GNC – Guidance, Navigation, and Control
HVA – High Value Asset
LiDAR – Light Detection and Ranging
RADAR – Radio Detection and Ranging
RFS – Random Finite Set
RPO – Rendezvous and Proximity Operations
RSO – Resident Space Object
SLAM – Simultaneous Localization and Mapping
SSA – Space Situational Awareness
UKF – Unscented Kalman Filter

1. INTRODUCTION AND MOTIVATION

Providing satellites with the autonomy to make intelligent decisions independent of an operator is a crucial enabler for future space operations. There is a particular need to advance the state-of-the-art in autonomous Guidance, Navigation, and Control (GNC) technology in support of space-based Space Situational Awareness (SSA) and orbital debris removal. In these missions, an autonomous inspector satellite needs to be able to detect, recognize, classify, and track resident space objects (RSO's) of interest, including their location, size, and shape. A critical and challenging question for such missions is the identification and characterization of the RSO being inspected via estimation of the object's shape. Ideally, a combination of vision-based, LiDAR, and RADAR would be used to characterize the object. However, when observations from vision-based cameras are excluded due to poor lighting conditions, the use of LiDAR and/or RADAR in conjunction with advanced estimation techniques can achieve accurate shape estimation.. LiDAR and RADAR sensors have the added benefit of providing ranging information as well as angle information and thus more information content than simply using angles-only.

The simultaneous localization and mapping (SLAM) problem has been solved with different sensor types through the innovations of self-driving cars and other robotic applications. A shape can be estimated with neural networks and point clouds, Bayesian estimation framework, and other methods. Additionally, there are numerous methods for

reconstructing the surface of an object to enhance the features of an object [1]. In this paper we will not be addressing the problem to estimate the location of the object or the surface reconstruction after the shape has been estimated. We will be focusing on a random finite sets (RFS) estimation approach for the estimation of extended objects. The RFS estimation approach is a powerful Bayesian framework that has been proven effective for estimating extended objects. An extended object is an object that produces multiple detections on the sensor, i.e. from a vision-based or flash-LiDAR sensor [4]. Vision based sensors provide measurements used to estimate the shape of an object, but have illumination constraints that hinder its applicability in non-ideal lighting conditions. LiDAR and RADAR sensors eliminate the need for the object to be illuminated. High-fidelity LiDAR sensor models have been developed for extended objects in rendezvous and proximity operations (RPO), and autonomous landing systems, and asteroid exploration missions [3, 6]. Using the RFS estimation approach with a high-fidelity sensor model, the shape of an object can be estimated. This paper then expands on the estimation framework to include an autonomous navigation to control the motion of the sensor around the object to estimate its shape.

This paper presents the fundamental research funded by Air Force Office of Scientific Research (AFOSR) to autonomously estimate the shape of an object using an RFS approach. In this paper, we outline the theory behind an RFS Bayesian estimation approach. This section derives the formulation of Bayes' law and provides an in-depth explanation of the likelihood of false alarms and missed detections, the predicted prior that includes birth and death, and the normalization factor from the measurement. We then develop the chosen implementations of RFS Bayesian framework to our specific problem for shape estimation. This section relates the RFS and Bayes' law to our chosen implementations of the likelihood, predicted prior, and normalization. Our implementation allows for the simultaneous update of birth, death, false alarms, and missed detections for all possibilities of associations while maintaining tractability. The underlying continuous Probability Density Function (PDF) representing each state are updated with using an Unscented Kalman Filter (UKF). After the update, the system's entropy is evaluated and used to influence the autonomous motion of the inspector satellite around the object.

The rest of the paper is structured as follows, the application scenario is described and details of the RFS shape estimation simulation are listed. We then show the results of two simulation scenarios where the shape of unknown objects are estimated. The final section discusses the results of the autonomous shape estimation and the steps for the continuation of the work presented in this paper.

2. SHAPE ESTIMATION

2.1. Problem Description

If an unknown RSO is in orbit, an inspector satellite can approach the RSO to determine if the RSO poses a potential threat by inferring its mission from resolved spatial features, size, and shape. Additionally, if there is a high value asset (HVA) in orbit, an inspector satellite could be used to evaluate the state of health of the HVA. Knowing the size and shape of the RSO is essential to determine if the RSO is dangerous or in a bad state of health. The inspector satellite would need to be within close proximity of the object in order to estimate the size and shape of the RSO. In these conditions, the inspector satellite needs to assess the object as efficiently as possible without the guarantee of object illumination and communication with the ground. An inspector satellite may have a variety of sensors on-board that could aid in characterizing the object, such as a vision-based sensor, but without the right lighting conditions or command, the overall characterization is limited. With a high-resolution LiDAR sensor, the RSO can be characterized in non-ideal lighting conditions. The LiDAR sensor provides azimuth, elevation, and range measurements of the object without the need for lighting. The shape estimation metrics are used to influence the autonomous maneuvering of inspector satellite around the RSO in proximity operations to fully characterize the object. The closed-loop feedback from the algorithm allows the inspector satellite to autonomously navigate and estimate the shape without the need for ground communication or a human-in-the-loop process. This combination of azimuth, elevation, and range measurements plus autonomy allow for the RSO size and shape to be efficiently determined to infer if the RSO presents a threat or if the HVA is in a bad state of health.

2.2. Core Bayesian Mathematical Formulation

To illustrate the core Bayesian mathematical formulation, consider an example of determining the correct shape of an RSO provided observations from an inspector satellite. There are many approaches to estimating shape. For this paper,

we have considered constructing the shape from a set of facets. The Bayesian approach will utilize the observations to refine our knowledge of the underlying states of the facets. First, consider the space $\mathcal{S} = \mathbb{R}^N$ that uniquely and exhaustively specifies the possible states of the physical facet aspects that are of interest. Next consider a random set, S, of facets containing a random number of facet states defined on $\mathcal{S}$,

$$S = \{s_1, s_2, \dots, s_n\}. \quad (1)$$

Where $s_i,\ i = 1,2, \dots n,$ are random vectors containing all continues and discrete physical aspects defining a facet. This may include position of the center point of the facet, velocity of the center point, orientation of the facet, shape, etc.

We can then define an observation space $\mathbb{Z} = \mathbb{R}^L$ that uniquely and exhaustively specifies the pieces of information that can be observed. Each measurement of the measurement set, $M^k = \{m_1, m_2, \dots, m_l\}$, received at time, k, from the surveying spacecraft is defined on $\mathbb{Z}$. Next we can then define integrable functions for the state transition model, observation model, and likelihood function as $p_{k+1|k}(S|S', M^k)$, $H(S)$, and $p_{k+1|k}(M^{k+1}|S)$. Each of these are stochastic in nature and contain the respective noise models. For some initialized distribution for a general time step, k,

$$p_{k|k}(S|M^k) = \rho(n) \sum_{\nu} \prod_{i}^{n} p_k(s_{\nu i}|M^k)\ w_\nu \quad (2)$$

in which $\rho(n)$ is the cardinality distribution and $p_k(s_{\nu i}|M^k)$ is the special distribution of the i^{th} facet. The variable ν represents all possible cardinality n subsets of S and w_ν represents the weight of that subset.

The update equation to properly combine the information from the measurement set, M^{k+1}, to update the predicted facet set, S, using Bayes law is,

$$p_{k+1|k+1}(S|M^{k+1}) = \frac{p_{k+1}(M^{k+1}|S)p_{k+1|k}(S|M^k)}{p_{k+1}(M^{k+1}|M^k)} \quad (3)$$

In this expression, $p_{k+1}(M^{k+1}|S)$ represents the likelihood expression of the measurement M^{k+1} given S and includes missed detection and false alarm processes $p(\emptyset|S)$ and $p_c(M)$. In this work, missed detections are modeled as a binomial process and false alarms are modeled as a Poisson process that is uniformly distributed in the region of consideration V. The likelihood expression used can then be written, leaving out time dependence for brevity, as follows,

$$p(M|S) = e^{\lambda} p_c(M) p(\emptyset|S) \sum_{\sigma} \prod_{i:\sigma(i)>0} \frac{p_d p(m_{\sigma(i)}|s_i)}{(1-p_d)\frac{\lambda}{V}} \quad (4)$$

Where σ represents all data association hypotheses. The clutter process and missed detection process are further expressed,

$$p_c(M) = e^{-\lambda} \prod_{m \in M} \frac{\lambda}{V} \quad (5)$$

and

$$p(\emptyset|S) = e^{-\lambda} \prod_{s \in S} (1 - p_d) \quad (6)$$

Such that p_d is the probability a facet is detected and λ is the clutter Poisson arrival rate.

The second term in the update expression is the predicted prior $p_{k+1|k}(S|M^k)$ and can be written in terms of the of the Markov transition density $p_{k+1|k}(S|S')$ to include facet birth and death.

$$p_{k+1|k}(S|M^k) = \int p_{k+1|k}(S|S') p_{k|k}(S'|M^k) \delta S' \quad (7)$$

In this work, the birth process is modeled as a Poisson process distributed uniformly in the region of consideration V while the death process is modeled as a binomial process. The Markov transition density can then be expressed, leaving out time dependence for brevity, as follows,

$$p(S|S') = e^{\lambda_B} p_B(S) p(\emptyset|S') \sum_{\theta} \prod_{i:\theta(i)>0} \frac{(1-p_D) p\left(s_{\theta(i)}|s_i'\right)}{p_D \frac{\lambda_B}{V}} \quad (8)$$

Where θ represents all possible predicted hypotheses. The birth and death processes can be represented,

$$p_B(S) = e^{-\lambda_B} \prod_{s \in S} \frac{\lambda_B}{V} \quad (9)$$

and

$$p(\emptyset|S') = e^{-\lambda} \prod_{s' \in S'} (1-p_D) \quad (10)$$

The main difficulty in implementing this formulation is computational complexity. In the following section, the implementation used to keep the shape estimation problem feasible is discussed along with explanations for any necessary assumptions.

2.3. Implementation of RFS Shape Estimation

As stated in the introduction, the goal of this paper is to provide a methodology capable of autonomously influencing the spacecraft GNC to estimate the shape of a target RSO. To achieve this goal we make a simplifying assumption so we may address heart of the autonomous shape estimation problem. The inspector satellite and RSO are assumed to already be in a controlled Rendezvous and Proximity Operations (RPO) scenario with no relative motion between the surveying satellite and the target RSO. This simplification allows us to verify that our approach to solving the shape estimation piece is performant. It also allows us to define a discrete set of maneuvers that describe the possible actions the surveying satellite may select to optimally survey the target RSO and determine its shape. Times that these actions are selected are determined in an autonomous fashion and are dependent on the current information state of the system. The RFS based formulation developed in the previous section can be solved many different ways. To keep the problem tractable we implemented a hypothesis perspective approach similar to [9]. This implementation allowed us to accurately model the stochastic processes involved in the shape estimation problem while being agnostic to the underlying state representation and corresponding continuous filter.

The state space considered for this application is, $\mathcal{S} = \mathbb{R}^N$, where $N = 3$. Where each state defined on the space consists of the Cartesian position of the center of the facet in the relative frame,

$$s_i = \begin{bmatrix} x_i \\ y_i \\ z_i \end{bmatrix}. \quad (11)$$

Each facet, s_i, evolves according to a stochastic differential equation of the following form,

$$\dot{s_i}(a_j) = f_{i,j}(s_i, a_j) + \nu. \quad (12)$$

Where $f_{i,j}(.)$ is a non-linear function that describes the motion of the facet, i, in the relative frame with respect to the, j^{th} action. Since it is assumed that the surveying object and the target object are fixed in the relative frame, the motion of the facet can be completely described by the action and the white noise process, ν. It is a desire of future research to embed the full GNC law into this stochastic equation, but it is not of particular importance for highlighting the contributions of this paper.

We assume that the surveying satellite is equipped with a single flash-LiDAR sensor that produces a sets of noisy observations, $M^k = \{m_1, m_2, \dots, m_l\}$, at each time, k, where the measurements, z_i exist in $\mathbb{Z} = \mathbb{R}^L$, and $L = 3$. Each measurement contains the azimuth, elevation, and range in the sensor's body frame. The relationship between the observation space and the state space is defined as,

$$m_i = h(S_i) + \omega, \quad (13)$$

where $h(.)$ defines the non-linear transformation between the Cartesian relative frame of the detected facet subset, S_i, and the observation space. ω is a white noise process. The measurement set creates a 3-D point cloud representation of the object in azimuth, elevation, and range.

For each discrete time step, we simulate a measurement of a flash-LiDAR system producing a set of returns of azimuth, elevation, and range in the sensor FOV. Due to the hypothesis perspective that approximates the full RFS based derivation in section one, we need to solve a Data Association Problem (DAP) to determine the permutations of measurement assignments to the predicted facets. For each hypothesis in our set of hypotheses, we create a data association matrix (DAM) that allows us to solve the DAP. The DAM allows us to account for both predicted hypotheses and joint data association hypotheses simultaneously. The DAM provides us the ability to generate the highly likely joint hypotheses without having to exhaustively generate all possible hypotheses. It is important to note that if one generated all possible hypotheses the resulting updated hypotheses would completely reconstruct the posterior finite set statistics (FISST) PDF, however the number of possible hypotheses is computationally intractable so the posterior PDF is approximated using a subset of the highly likely hypotheses. This approximation keeps the problem tractable and is accomplished by utilizing the DAM to implement Munkres' or Murty's K-Best algorithms. Equations 14 – 18 are used to populate the DAM. The likelihood for facet, i, according the joint data association and predicted hypothesis vi can be expressed.

$$p_{k+1}\left(m_j{}^{k+1} \middle| s_{vi}, M^k\right) = \frac{1}{\sqrt{2}\pi|B|} e^{\frac{1}{2}\left(m_j - \widehat{m_{vi}}\right)^T B^{-1} \left(m_j - \widehat{m_{vi}}\right)^T}. \quad (14)$$

In which, B is the combined state and measurement covariance.

The probability of birth, death, false alarms, and missed detections can be expressed as the following.

$$p_B(S) = p_B * p_d * (1 - p_c) * b \quad (15)$$
$$p(\emptyset|S') = p_D * (1 - p_d) \quad (16)$$
$$p_c(M) = (1 - p_d) * p_c * (1 - p_B) * c) \quad (17)$$
$$p(\emptyset|S) = (1 - p_d) * (1 - p_D) \quad (18)$$

Where b and c are user defined values that represent the spatial-temporal Poisson distribution. These values are tuned to keep the probability of birth and clutter on the same order of magnitude as the likelihood of the joint data association. In a sense we are tuning the b and c values to approximate the Poisson processes assuming a Poisson arrival and a spatial distribution equivalent to a Gaussian centered at the assigned measurement m. Further description of this approach can be found in [9].

The normalized weight of each hypothesis can then be represented as the discrete portion of the update,

$$w_{i,j} = \frac{w_i l(j|i)}{\sum_{(I,J)} w_I l(J|I)}. \quad (19)$$

The underlying continuous spatial density of each facet is updated using an Unscented Kalman Filter (UKF) [10]. The result is an updated hypothesis from the measurement with a normalized weight.

To perform shape estimation in an autonomous fashion, an intelligence must be embedded within the core functionality to determine both when to take a maneuver action and also which maneuver action to take. To aid in explaining how the autonomous process is performed, we introduce the idea of the information state of the system, $\chi(k)$, at any time, k. The information state of the system can be completely described by the RFS based multi-facet PDF. The embedded intelligence uses an understanding of the information state to make decisions on what to do and when to do it. This is done by monitoring the deviations in information state, ΔI(χ(k),M(k)) that occur after a measurement is received. ΔI(.), also known as the incremental information gain, can be quantified in terms of various functions of the information state and a measurement set. For this paper, we quantify the information gain as the average change in system entropy. The entropy for a Gaussian facet PDF can be written,

$$E_l = \frac{1}{2}\, log(|P_l\,|(2\pi e)^N). \quad (20)$$

Where $|P_l\,|$ is the determinant of the l^{th} facet covariance. The total entropy of the maximum a posteriori hypothesis, H^*, is then the summation over all facets, j, such that $j \in H^*$. The change is then simply the different of the total entropy before and after the measurement update. The differential entropy of a hypothesis used to determine if the sensor should maneuver. If the differential entropy remains relatively constant after measurement updates, the system will make the decision on whether or not to maneuver. This decision is made by determining which action has the most potential for information gain. This can be framed as an optimization problem over the action space. Taking advantage of the fact that $M(k)$ is dependent on which action is selected, the information gain can be written $\Delta I(a(k))$. The optimization problem can then be expressed,

$$\max_{(a(k))} J(\chi(k)) = \max_{(a(k))} \Delta I\,(a(k).) \quad (21)$$

Determining the optimal action, a^*, that maximizes the information gain over all possible actions is extremely difficult if we considered a(k) to be a continuous action space, however, due to our early assumption of a fixed relative pose we can define a discrete set of actions that makes this optimization problem straightforward. For instance, it is often solvable using an exhaustive search. This recursive framework is continued until a single hypothesis has converged and the shape of the object has been estimated. Once the shape has been estimated, the shape can be reconstructed through various methodologies to extract defining features [1]. The focus of this paper is on the shape estimation and autonomy, but reconstruction is considered in future work.

3. APPLICATION AND SIMULATION

3.1. Application

An overview of the shape estimation scenario can be seen in Fig. 1. In this scenario, an inspector satellite is orbiting around and unknown RSO or HVA in RPO conditions with the intent to autonomously maneuver around the RSO to estimate the shape.

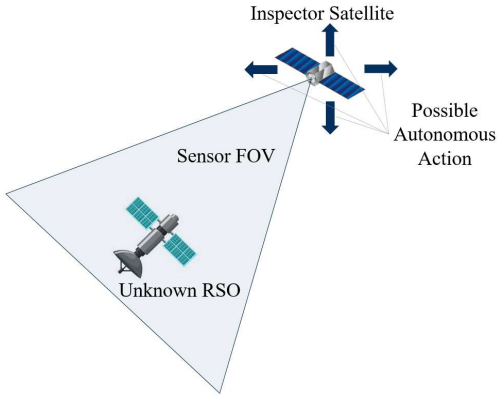

Figure 1

The inspector satellite and RSO positions and orientations are defined in a pseudo-inertial frame. The inspector satellite has possible autonomous actions that it can take based to maneuver around the object in the pseudo-inertial frame. The inspector satellite has 6 pre-defined maneuvers to move $\pm$ a specified distance in the X, Y, and Z directions. This simplification assumes the position and orientation of the RSO is known and the GNC law of the inspector satellite maintains no relative motion between the inspector and RSO. In future work, we would like to include the estimation of the position and orientation, in addition to the autonomous shape estimation of the RSO. The RSO has a fixed location and orientation located at the origin of the pseudo-inertial frame. The inspector satellite is located within range of proximity operations of less than 1 km [6].

The LiDAR sensor is mounted along the X-Body axis of the inspector satellite. The inspector satellite is orientated to have the X-Body axis aligned with the center of the RSO. The LiDAR sensor used in the simulation is a flash-LiDAR sensor. The flash-LiDAR system illuminates a scene with a single pulse, and on upon receiving the pulse each detector pixel records the time taken to receive the signal from the target. This pulse results in a set of azimuth, elevation, and range measurements that represent a point-cloud representation of the object. The sensor parameters used to model our flash-LiDAR sensor are comparable to other RPO LiDAR missions, such as Autonomous Landing Hazard Avoidance Technology (ALHAT) [7].

As the inspector satellite autonomously maneuvers around the unknown RSO taking LiDAR measurements, the shape of the object is estimated. After the shape has been estimated, the shape could be reconstructed to define the feature of the object. With a known shape, the unknown RSO and HVA can be assessed as a potential threat or evaluated for damage.

3.2. Simulation

The shape estimation simulation is a discrete time-based simulation. At each discrete time-step, a measurement is simulated. The measurement is simulated by first transforming all of the facets of the object into the measurement space of the sensor. Then for each pixel, the facets are evaluated to determine if any facet is within the FOV of the pixel. If the facet is within the FOV of the pixel, the range from the center of the pixel to the object is determined. The result is a set of azimuth, elevation, and range measurements of the object if the FOV of the sensor. A white noise process is added to the measurements on the order of arc-seconds and centimeters. In addition to adding noise to the measurements, a Poisson process is used to generate false alarm detections. An example of a simulated LiDAR measurement of a single side of a cube can be seen in Fig. 2. The false alarms generated cannot be seen in this view, to better show the noise in the range of the measurements.

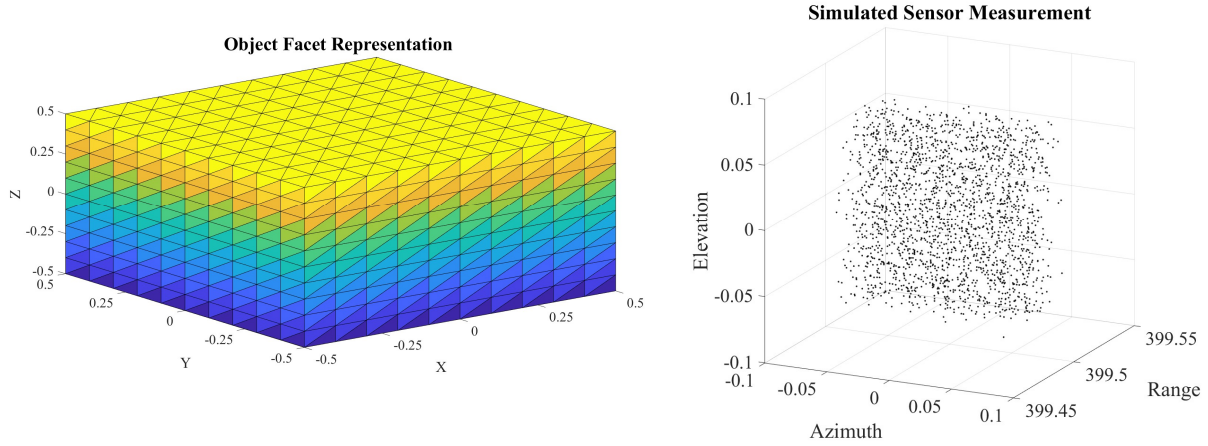

Figure 2

The initial hypothesis passed to the recursive framework is an empty set from no a-priori information about the object. In the recursive framework, at each discrete time-step, a measurement of the object is simulated. For each hypothesis, we solve the DAP with the measurements using the DAM. The DAM is created using the likelihood of association from a facet to a measurement, probability of birth, death, false alarm, and missed detections, as shown in equations 15-18, respectively. In order to solve for the likelihood of joint association, the hypothesis facets need to be transformed into the measurement space. The DAM is then solved with Munkres' and Murty's K-Best solutions. Munkres' solution provides the Hungarian of the DAM and Murty's K-Best provides K number of slightly perturbed versions of the Hungarian associations. For each of the Murty's K-Best solutions the hypothesis is updated. The joint associations are updated with a UKF. The birth and false alarm associations are added to the hypothesis, and the death and missed detection associations are removed from the hypothesis. The weight of the hypothesis is found from the

product of the probability of associations from DAM. The weights of the updated hypotheses created by the K-Best solutions are then normalized. This update process is repeated for each hypothesis within the set of hypotheses.

Once all of the hypotheses have been updated from a single measurement. Their weights are sorted and then pruned to leave only the 10 highest weighted hypotheses. The weights are again normalized. These hypotheses are then evaluated to determine the amount of entropy in the system as defined by Equation 20. If the differential entropy from the previous time steps is relatively constant, then we want to maneuver to a new location to increase the total information of our system. If the differential entropy is not constant, then we want to stay at our current location to continue to gather information. The system has pre-defined maneuvers in the pseudo-inertial frame to evaluate which direction would provide the highest information gain into the system. The pre-defined maneuvers are limited to keep the range of the inspector satellite and the object within a certain threshold and to only new positions. This prevents the autonomy from moving the sensor too close or too far and not returning to the same location. After all pre-defined maneuvers are evaluated, the highest change in entropy maneuvers is selected and the sensor is moved to the new location. The hypotheses are then propagated to the next time step. This concludes a single iteration of the recursive framework. Figure 3. 3 outlines the steps previously described of the RFS Bayesian Recursive Framework.

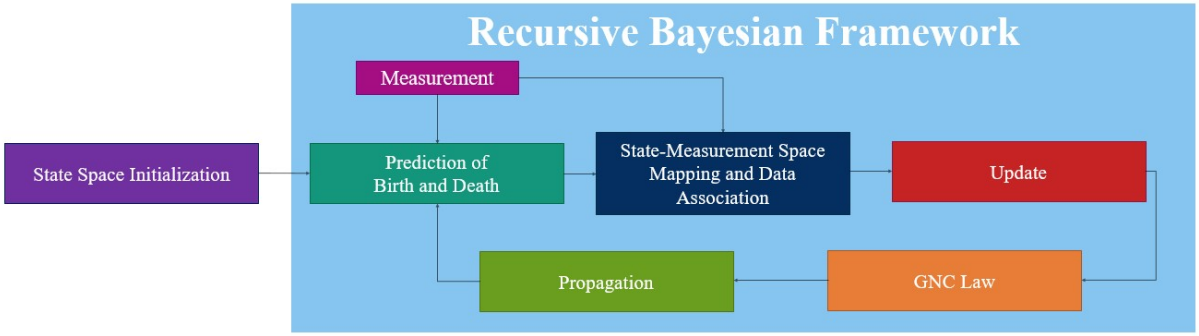

Figure 3

The framework is exercised until the shape of the object is estimated. Once the shape of the object is estimated, many techniques are available to reconstruct the shape of the object to provide more detail of the features. We did not utilize any of these techniques in this paper, but would like to include shape reconstruction in future work.

3.3. Simulation Results

A shape estimation scenario was presented with an inspector satellite with a LiDAR sensor and the capability to autonomously maneuver around an unknown object and estimate the shape. Two simulations scenarios are presented in this paper. In the first simulation the inspector satellite autonomously estimated the shape of an unknown object, a simple 1 m^3 cube, shown in Fig. 2. The second simulation shows the shape estimation results of estimating the shape of NASA's Advanced Composition Explorer (ACE). The ACE spacecraft shape definition was loaded into the simulation and transformed into triangular facets. The facet representation and actual ACE spacecraft can be seen in Fig. 7 [11]. The shape of the "unknown" object in the first simulation was estimated with the RFS Bayesian recursive framework presented in this paper. As the inspector satellite maneuvers around the object, the shape of the object is formed. Fig. 4 shows the evolution of the shape as the shape is estimated. False alarms are present in the hypothesis, but not all are visible in the view presented.

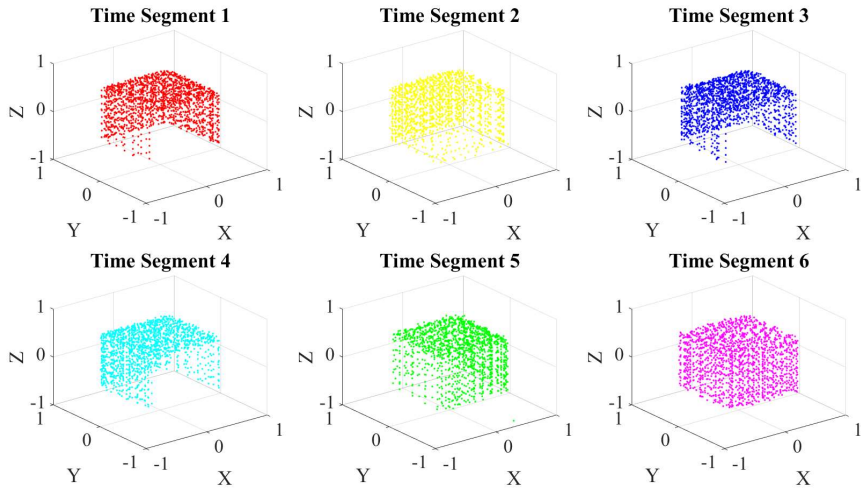

Figure 4

As the inspector satellite maneuvers around the object the shape becomes more defined and can clearly be defined as a cube. Each color represents a time segment of the hypothesis. Each graph shows $1/6^{th}$ of the time to estimate the shape of the object. The final estimate of the object can be seen in Fig. 5.

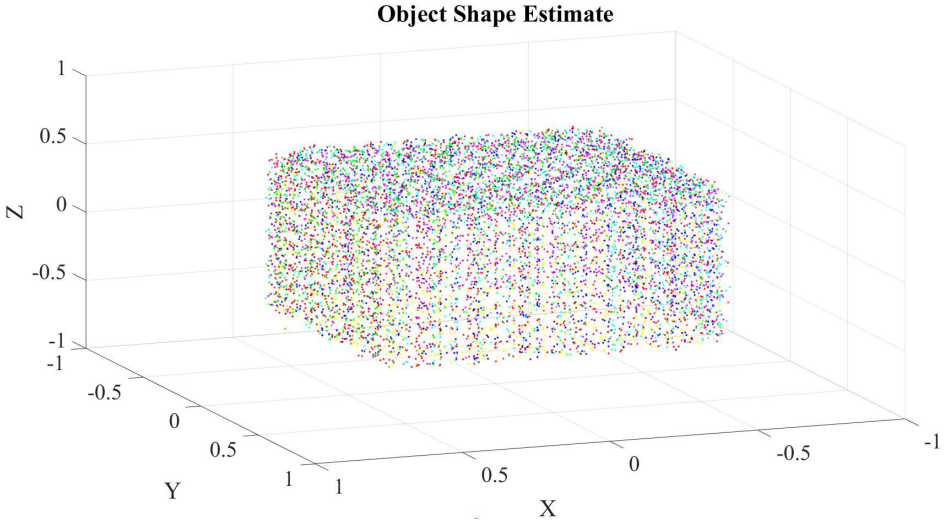

Figure 5

The relative path of the satellite in the pseudo-inertial frame is shown in Fig. 6. Each colored dot represents the location where a measurement was taken. The color of the sensor position is consistent with the colors shown in Fig. 4, which are broken into six time segments. As shown, the inspector satellite starts where the red dots are located, and as more information is learned, maneuvers around the object where the shape estimation process is completed with the pink dots.

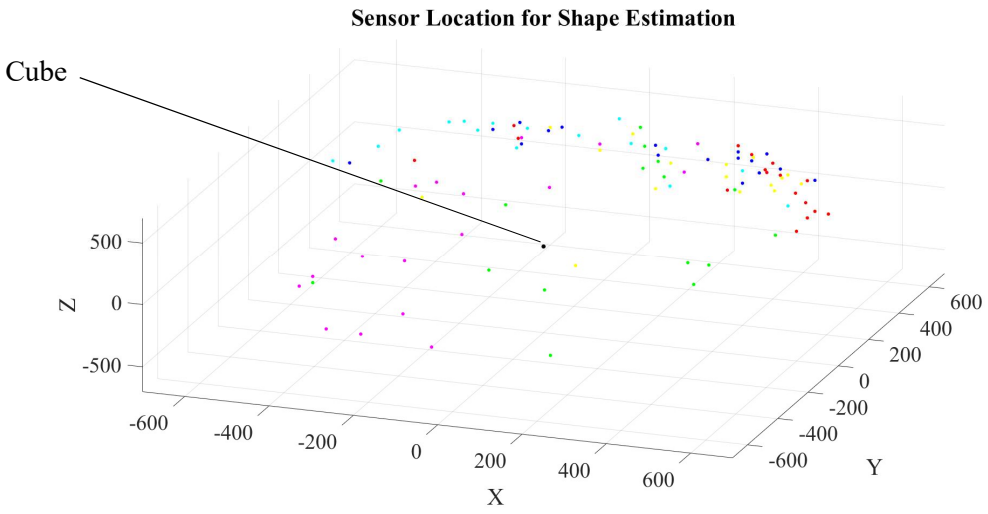

Figure 6

The path shows how the inspector satellite autonomously maneuvered around the object to estimate the shape. The inspector satellite maneuvered in the direction of the highest entropy gain to the system based on the pre-defined maneuvers.

The second simulation scenario, of ACE, shows the estimation of features of an object. Fig. 7 shows ACE which has four large extended solar panels, two of which have extended booms with mag sensors. The body of the spacecraft has various instrumentation designed to understand the evolution of the solar system [11].

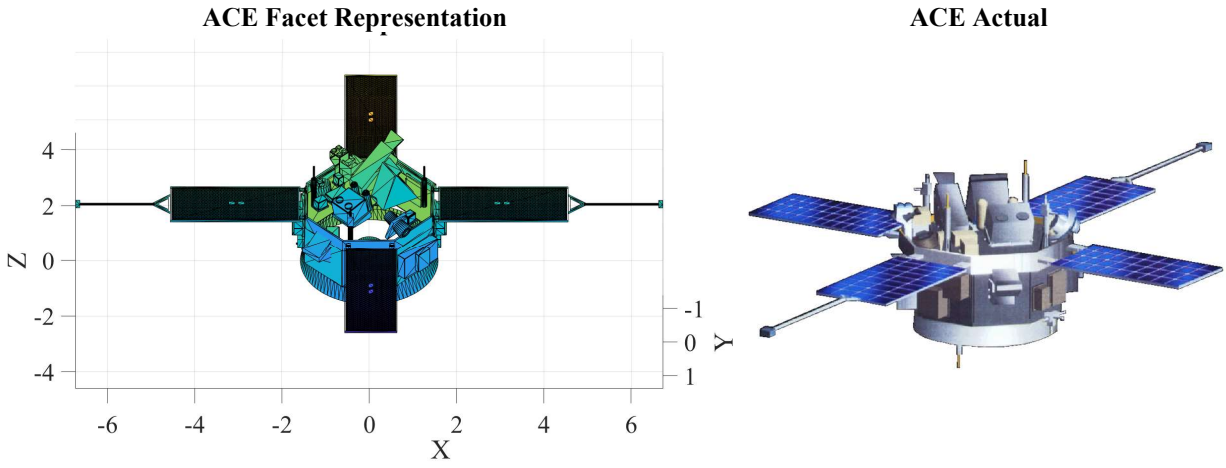

Figure 7

The simulation was conducted with the same sensor parameters, but the operating distance was adjusted to maintain the entire ACE spacecraft within the FOV. The simulation was able to accurately estimate the shape of the object such that you can recognize features. These features could be enhanced more with a shape reconstruction methodology. Fig. 8 shows the time history of the shape estimation.

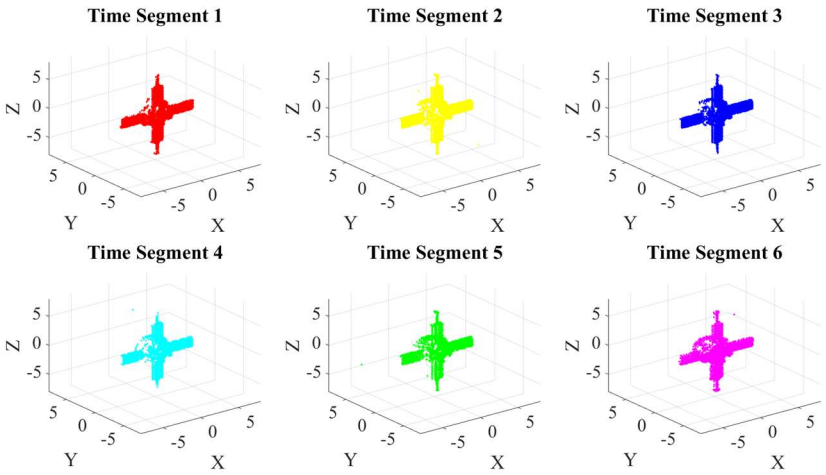

Figure 8

Fig. 9 shows the final shape estimated. The details of the spacecraft, such as the mags are clearly visible, even early on in the shape estimation. The other instrumentation on the body of the satellite can be discerned from the shape. This is important information that can be used to characterize the satellite.

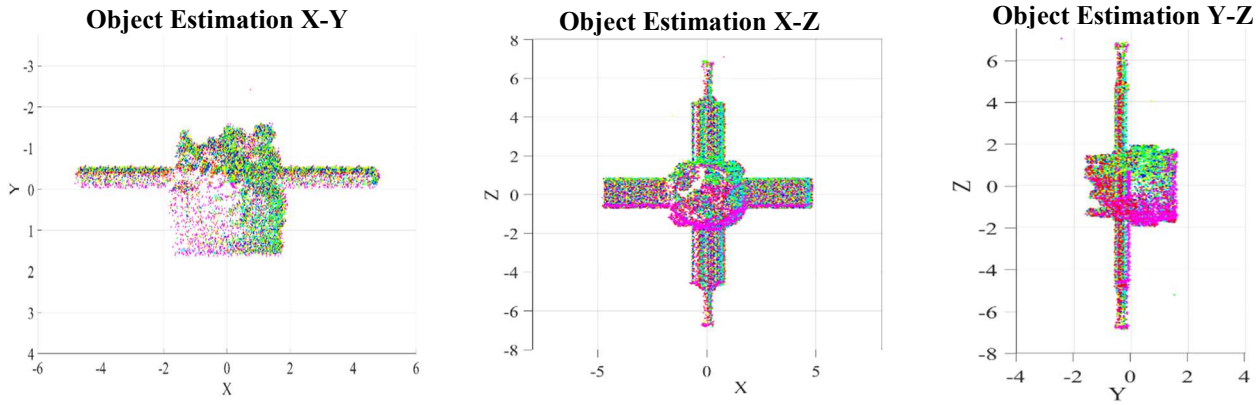

Figure 9

Finally, we can visualize how the inspector satellite autonomously maneuvered around the ACE spacecraft to fully estimate the shape in Fig. 10. The color of the dots represent the time segment from which the measurement was taken.

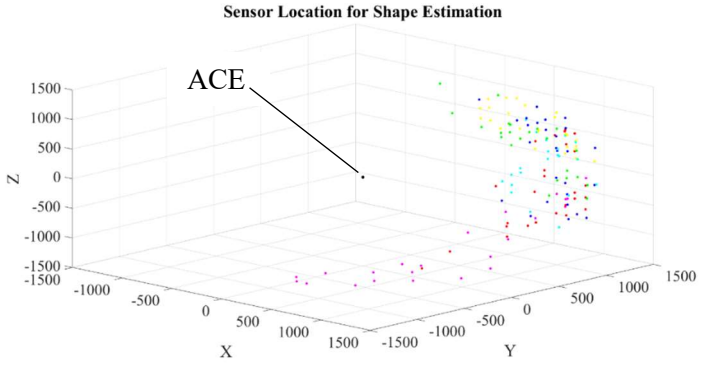

Figure 10

The inspector satellite at first stays within a small region but as more information about the system is known, it maneuvers outside of the small region to complete the shape estimation. Both simulations were able to successfully estimate the shape of an "unknown" object with a LiDAR sensor through autonomous motion.

4. SUMMARY, CONCLUSION, AND FUTURE WORK

4.1. Summary and Conclusion

In this paper, we provided the theory behind a RFS Bayesian estimation framework. We expanded on the theory to include our specific implementation details for shape estimation. Then, the details of the application and simulation along with the simulation results of an inspector satellite autonomously estimating the shape of an unknown objects were presented. The proposed framework estimated the shape of an unknown objects based on an autonomous control of the inspector satellite around the object.

4.2. Future Work

As a continuation to the work outlined in this paper, we would like to include the SLAM problem solving to include the estimation of the position and orientation of the object. This would allow us to create a more advanced GNC law to control the relative motion between the inspector satellite and RSO. From this, we could explore additional optimizations of a continuous maneuver space. Additionally, we would like to add in a post-processing shape reconstruction functionality to extract features from the unknown object. For example, we could reconstruct the shape of the ACE satellite to better determine the type of instrumentation on the body of the spacecraft. Other areas of research would include evaluating different sensor parameters and their effect on shape estimation and creating metrics for the effectiveness of estimating the shape of an object.

5. ACKNOWLEDGEMENTS

We would like to thank the leadership from L3Harris – Applied Defense Solutions (ADS) for their support in the research presented in this paper, especially Thomas Kelecy. We are also grateful for AFOSR for the invaluable support allowing for this research to be completed.

6. REFERENCES

[1] L. Stephen, A. Jose, "An Overview of Surface Tracking and Representation in Fluid Simulation"m in International Journal of Advanced Computer Science and Applications (IJACSA), vol. 6, no. 11, 2015.
[2] F. Aghili, M. Kuryllo, G. Okouneva, C. English, "Fault-Tolerant Position/Attitude Estimation of Free-Floating Space Objects Using a Laser Range Sensor", in IEEE Sensors Journal, Vol. 11, No. 1, pp. 176-185, January 2011.
[3] A. Rathinam, A. Dempster, "3D Reconstruction of an Asteroid Using Visual SLAM for Autonomous Navigation", in 17th Australian Space Research Conference (ASRC), November 2017.
[4] K. Granstrom, C. Lundquist, F. Gustafsson and U. Orguner, "Random Set Methods: Estimation of Multiple Extended Objects," in IEEE Robotics & Automation Magazine, vol. 21, no. 2, pp. 73-82, June 2014.
[5] Karl Granstrom, Marcus Baum, Stephan Reuter, "Extended Object Tracking: Introduction, Overview and Applications," arXiv: 1604.00970, URL: https://arxiv.org/abs/1604.00970.
[6] J. Christian, S. Cryan, "A Survey of LIDAR Technology and its Use in Spacecraft Relative Navigation", in AIAA, URL: https://ntrs.nasa.gov/archive/nasa/casi.ntrs.nasa.gov/20140000616.pdf.
[7] F. Amzeajerdian, L. Petway, G. Hines, V. Roback, R. Resisse, D. Pierrottet, "Lidar Sensors for Autonomous Landing and Hazard Avoidance", in AIAA, URL: https://ntrs.nasa.gov/archive/nasa/casi.ntrs.nasa.gov/20140002742.pdf.

[8] G.D. Hines, D.F. Pierrottet, F. Amzajerdian, High-Fidelity Flash Lidar Model Development, SPIE 9080, SPIE Defense and Security Symposium, Baltimore, MD, 2014, 5 – 9 May.
[9]W. Faber, "Multiple Space Object Tracking Using A Randomized Hypothesis Generation Technique", in Dissertation to the Office of Graduate and Professional Studies of Texas A&M University, URL" http://hdl.handle.net/1969.1/173387.
[10] S. Julier, J. Uhlmann, "A New Extension of the Kalman Filter to Nonlinear Systems", in *Int. Symp. Aerospace/Defense Sensing, Simul. And Controls*. Signal Processing, Sensor Fusion, and Target Recognition VI. **3**: 182.
[11] Advanced Composition Explorer (ACE), in NASA 3D Resources, in URL: https://nasa3d.arc.nasa.gov/detail/ace and http://cse.ssl.berkeley.edu/stereo_solarwind/mission_ACE.html